MDPI

Article

Hybrid Xerogels: Study of the Sol-Gel Process and Local Structure by Vibrational Spectroscopy

Guillermo Cruz-Quesada [1,2], Maialen Espinal-Viguri [1,2,*], María Victoria López-Ramón [3] and Julián J. Garrido [1,2,*]

1   Departamento de Ciencias, Campus Arrosadía, Public University of Navarre (UPNA),
    31006 Pamplona, Spain; guillermo.cruz@unavarra.es
2   Institute for Advanced Materials and Mathematics (INAMAT[2]), Campus Arrosadía, Public University of
    Navarre (UPNA), 31006 Pamplona, Spain
3   Departamento de Química Inorgánica y Orgánica, Facultad de Ciencias Experimentales, University of Jaén,
    23071 Jaén, Spain; mvlro@ujaen.es
*   Correspondence: maialen.espinal@unavarra.es (M.E.-V.); j.garrido@unavarra.es (J.J.G.);
    Tel.: +34-948-169604 (M.E.-V.); +34-948-169601 (J.J.G.)

Abstract: The properties of hybrid silica xerogels obtained by the sol-gel method are highly dependent on the precursor and the synthesis conditions. This study examines the influence of organic substituents of the precursor on the sol-gel process and determines the structure of the final materials in xerogels containing tetraethyl orthosilicate (TEOS) and alkyltriethoxysilane or chloroalkyltriethoxysilane at different molar percentages (RTEOS and ClRTEOS, R = methyl [M], ethyl [E], or propyl [P]). The intermolecular forces exerted by the organic moiety and the chlorine atom of the precursors were elucidated by comparing the sol-gel process between alkyl and chloroalkyl series. The microstructure of the resulting xerogels was explored in a structural theoretical study using Fourier transformed infrared spectroscopy and deconvolution methods, revealing the distribution of $(SiO)_4$ and $(SiO)_6$ rings in the silicon matrix of the hybrid xerogels. The results demonstrate that the alkyl chain and the chlorine atom of the precursor in these materials determines their inductive and steric effects on the sol-gel process and, therefore, their gelation times. Furthermore, the distribution of $(SiO)_4$ and $(SiO)_6$ rings was found to be consistent with the data from the X-ray diffraction spectra, which confirm that the local periodicity associated with four-fold rings increases with higher percentage of precursor. Both the sol-gel process and the ordered domains formed determine the final structure of these hybrid materials and, therefore, their properties and potential applications.

Keywords: ORMOSILs; xerogels; hybrid materials; chloroalkyltriethoxysilanes; inductive effect; $(SiO)_x$ structures; FTIR

1. Introduction

Organically modified silicon xerogels (ORMOSILs) are attracting considerable interest for their application in new-generation technologies, being utilized in chemical and optical sensors [1–6], for catalysis [4,5], in coatings [6–10], for chromatography [11,12], and in pharmacy [13]. They have great chemical versatility and can be efficiently modified for specific applications due to their combination of highly varied mechanical, optical and textural properties [14].

The sol-gel method is the most widely used approach to the synthesis of hybrid silicon xerogels. It is based on co-condensation between monomers of traditional alkoxides $(Si(OR)_4)$ such as tetramethoxy- or tetraethoxysilane (TEOS and TMOS, respectively) and one or more mono-, di- or trialkylsilanes $(R_xSi(OR')_{4-x})$ [15]. In hybrid xerogels, the addition of organic molecules or functional groups in the silica network restricts the three-dimensional growth of the material and blocks a condensation position, favoring the preferential formation of $(SiO)_4$ and $(SiO)_6$ rings in the amorphous structure of the silica

materials [16,17] and even leading to the formation of structures with a higher degree of order [18]. However, although the sol-gel process has been widely studied [19], some questions have yet to be adequately settled. For instance, multiple reactions take place simultaneously in the process, making it difficult to extract information from experimental procedures [20]. To date, many studies have attempted to elucidate the influence of precursors on the hydrolysis, condensation reactions, and crosslinking by applying different characterization and analysis techniques, including gas chromatography (GC) [21], nuclear magnetic resonance ^{29}Si NMR [22,23], Raman spectroscopy [24], and Fourier transform infrared spectroscopy (FTIR) [25,26]. Among these approaches, FTIR not only provides complementary information on the bonds and structures formed during the synthesis process but also, when combined with deconvolution methods, yields valuable data on the microstructure of siliceous materials [27–29]. Knowledge obtained by these means is of major interest because it allows for the prediction of: (i) the physical properties of xerogels derived from their structure [30]; (ii) the catalytic activity of metals supported in silica matrices [31]; and (iii) the correlation of the silica species in the membrane of a fiber optic sensor with its efficacy [32].

The ultimate application of these materials is as membranes in fiber optic sensors, on which the analyte is specifically and reversibly adsorbed. Physisorption of the analyte on the surface of the material generates a modification of the refractive index and produces a change in the reflected optical power, which determines the analyte concentration in the medium. For this reason, it is important to prepare materials with different porosities and surface chemistries in which the interaction between the membrane (chemical area of a sensor) and the analyte is specific and labile. To date, our research group has prepared membranes with hybrid xerogels obtained using different molar ratios of TEOS:RTEOS (R = methyl or phenyl) [33,34]. Given the results obtained and following this line of reasoning, the addition of a chlorine atom to the organic moiety of a silane emerged as a highly appealing approach because of the inductive effects of the chlorine, which generates a more active chemical surface and favors functionalization with other compounds. For these reasons, ClRTEOS precursors were used to synthesize three series of xerogels analogous to those prepared in previous studies [35].

The objective of this study was to determine the influence of the alkyl and chloroalkyl substituents of the precursors on: (i) the gelation time, and (ii) the microstructure of the synthesized materials, obtained by deconvolution of the FTIR spectra. The study used six series of hybrid xerogels prepared (in previous studies) with tetraethoxysilane (TEOS) and a chloroalkyl or alkyl precursor at different molar percentages (ClRTEOS or RTEOS: R = methyl [M], ethyl [E]; and propyl [P]) [35–38]. Theoretical study of the deconvolution of the band at 1300–980 cm^{-1} in the FTIR spectra yielded semi-quantitative information on the proportion of $(SiO)_4$ and $(SiO)_6$ rings related to periodic structural domains and amorphous silica, respectively. This allows the local internal order of materials to be determined and the influences of the organic substituent and chlorine atom to be predicted. The ultimate application of these materials is as membranes in fiber optic sensors, constituting the chemical area of the sensor, where the analyte is specifically and reversibly adsorbed. Physisorption of the analyte on the surface of the material generates a modification of the refractive index and produces a change in the reflected optical power, which determines the analyte concentration in the medium. This study is of crucial importance because: (i) precise knowledge of the gelation time is essential to effectively impregnate the fibers [33,34], and (ii) complete characterization of the xerogels allows prediction, to a large extent, of their properties and the a priori selection of the xerogel best suited to the characteristics of the analyte of interest [32].

2. Materials and Methods

2.1. Materials

The siliceous precursors TEOS (tetraethoxysilane, purity > 99%), ClMTEOS (chloromethyl)triethoxysilane, purity > 95%), and ClPTEOS ((3-chloropropyl)triethoxy silane, pu-

rity > 95%) were supplied by Sigma-Aldrich (San Luis, MO, USA), and ClETEOS ((2-Chloroethyl)triethoxysilane, purity > 95%) was obtained from Fluorochem (Glossop, UK). Absolute ethanol (Emsure®) and hydrochloric acid (HCl, 37% w/w) were purchased from Merck (Darmstad, Germany) and potassium bromide (FT-IR grade) from Sigma-Aldrich (San Luis, MO, USA). All chemicals were used without further purification.

2.2. Synthesis of the Xerogels

The three series of hybrid xerogels were prepared as previously described [35–38]. TEOS was mixed with ClRTEOS (R = Methyl [M], Ethyl [E] or propyl [P]) at different molar ratios, maintaining a constant (TEOS + RTEOS):ethanol:water ratio (1:4.75:5.5) throughout the series.

The reagent and solvent quantities were adjusted to obtain 20 mL of alcogels. First, TEOS and ClRTEOS were mixed in a 30 mL container (φ 3.5 cm, threaded plastic lid, Schrarlab, Barcelona, Spain). Absolute ethanol was then added, followed by the dropwise addition of Milli-Q grade water under magnetic stirring to facilitate miscibility. Once the pH of the mixtures remained unchanged (after ~10 min), an automatic burette (Tritino mod. 702 SM, Metrohm, Herisau, Switzerland) was used to set the pH at 4.5 (0.05 M solution of HCl), and the mixture was stirred for 10 min to ensure homogenization. The closed containers were placed in a thermostatized oven at 60 °C (J.P. Selecta S.A, Barcelona, Spain) until gelling, i.e., when the shape of the materials did not change when the container was tilted. Subsequently, 5 mL of ethanol were added to cure the alcogel at room temperature for one week. Next, the containers were opened and covered with paraflim™, which was pierced with holes to facilitate evaporation of the solvent, and were then dried at room temperature under atmospheric pressure. The monolith was considered dried when no significant variation in its mass was observed. Finally, the xerogels were further dried (90 °C under vacuum) and then ground in an agate mortar.

2.3. Characterization

Infrared spectra were recorded using a FTIR spectrometer (Jasco, mod. 4700, Tokyo, Japan) at 25 scans and resolution of 4 cm^{-1}. Compressed KBr tablets with two different concentrations of sample were prepared: (i) 0.6 mg sample in 200 mg KBr tablet for spectra in the range 2200–400 cm^{-1}, thereby avoiding saturation of the Si-O-Si asymmetric stretching signal [39]; and (ii) 2 mg sample in 200 KBr tablet for spectra in the range 4000–2200 cm^{-1} for recording O-H and C-H bonds in greater detail. After their preparation, the tablets were dried over-night in an oven at 115 °C under vacuum to remove adsorbed water. Comparison between functional groups of the precursors in the pure reactant versus xerogel was carried out by using attenuated-total reflectance (ATR) to record the spectra directly from droplets of the precursors. The recorded transmittance of the samples was transformed into Kubelka-Munk units with the spectrometer software (Spectramanager, SMII FTIR Rev 216A ver2.15A) to allow their deconvolution (curve fitting) by a previously reported method [27]. Study parameters were four or five Gaussian-Lorentzian bands, with a maximum of 200 interactions, fixed baseline and >0.1 difference between experimental and synthetic spectra.
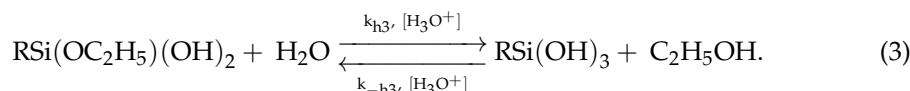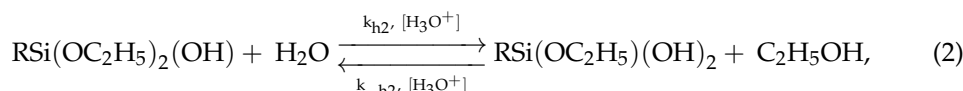
X-ray diffraction spectra were obtained at room temperature using a PANanalytical Empydrean XRD instrument (Empyrean, Almelo, The Netherlands) with graphite monochromator (at 45 KV and 40 mA) and copper rotating anode to select the CuK$_{\alpha1/2}$ wavelength at 1.54 nm. Measurements were performed in a stepped scan mode of $2 \leq 2\theta \leq 50°$ in steps of 0.013° at a rate of 0.5 steps s^{-1} [40].

3. Results and Discussion

3.1. Influence of Organochlorine Substituents on Gelation Time

The gelation time is the period between the initial mixture of reagents and the formation of the gel; it comprises hydrolysis, condensation, and gelation (stabilization of colloids and crosslinking) stages, with gelation being the limiting stage [41]. Density functional

theory (DFT) studies of TEOS in acidic media showed that the overall process of hydrolysis presents a pseudo-first order mechanism (SN_1) with lesser energy barriers in comparison to condensation [20]. Moreover, each consecutive hydrolysis reaction presents a barrier with less energy, which is consistent with the hydrolysis rates observed in ^{29}Si NMR experiments on various organoalkylsilanes [23]. The hydrolysis reactions of RTEOS are described in the following equations:

$$RSi(OC_2H_5)_3 + H_2O \xrightarrow{k_{h1}, \, [H_3O^+]} RSi(OC_2H_5)_2(OH) + C_2H_5OH, \qquad (1)$$

$$RSi(OC_2H_5)_2(OH) + H_2O \underset{k_{-h2}, \, [H_3O^+]}{\overset{k_{h2}, \, [H_3O^+]}{\rightleftharpoons}} RSi(OC_2H_5)(OH)_2 + C_2H_5OH, \qquad (2)$$

$$RSi(OC_2H_5)(OH)_2 + H_2O \underset{k_{-h3}, \, [H_3O^+]}{\overset{k_{h3}, \, [H_3O^+]}{\rightleftharpoons}} RSi(OH)_3 + C_2H_5OH. \qquad (3)$$
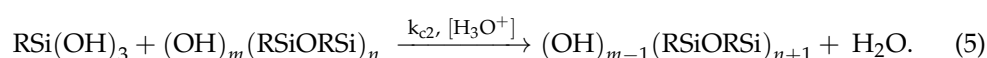
Reaction rates in the acidic hydrolysis of triethoxysilanes depend on the competition between the steric hindrance and inductive effects of the organic moieties [16]. The reaction rate decreases with an increase in the volume of the organic moiety [42], while electron donating groups (^+I) stabilize the pentacoordinated transition state and increase the electronic charge of the ethoxide in the hybrid precursor, facilitating the attack of the acidic proton (reactions 1–3) [20,43]. In previous studies, it was confirmed that the hydrolysis rates increase with a longer alkyl chain in the precursor due to the enhanced inductive effect of the moieties [23]. Given that chloroalkyltriethoxysilanes contain chlorine, an electron withdrawing group (^-I), hydrolysis rates are expected to be lower than their non-chlorinated analogs, as can be deduced from the partial charges of the ethoxide groups (δ_{OEt} values of Table 1).

Table 1. Electronegativities and partial charges of the chloroalkyl precursors and their alkyl analogs calculated from the Pauli electronegativities and application of the equations of Livage and Henry [44].

Precursor	R	X	δ_{Si}	δ_R	δ_{OEt}
TEOS	OC_2H_5	2.32	0.32	-	−0.08
MTEOS	CH_3	2.29	0.31	0.20	−0.17
ETEOS	C_2H_5	2.29	0.31	0.28	−0.20
PTEOS	C_3H_7	2.28	0.30	0.35	−0.22
ClMTEOS	CH_2Cl	2.32	0.32	−0.09	−0.08
ClETEOS	C_2H_4Cl	2.31	0.32	0.02	−0.11
ClPTEOS	C_3H_6Cl	2.30	0.31	0.11	−0.14

X, molecule electronegativity; δ, partial charge.

However, the condensation reactions determine the overall speed of the gelation process. The following equations exhibit the SN_2 mechanism for the first and consecutive acidic condensation reactions of RTEOS:

$$RSi(OH)_3 + RSi(OH)_3 \xrightarrow{k_{c1}, \, [H_3O^+]} OH-RSi(OH)-O-RSi(OH)-OH + H_2O, \quad (4)$$

$$RSi(OH)_3 + (OH)_m(RSiORSi)_n \xrightarrow{k_{c2}, \, [H_3O^+]} (OH)_{m-1}(RSiORSi)_{n+1} + H_2O. \quad (5)$$

In contrast to the hydrolysis reactions (Reactions 1–3), the first condensation between hydrolyzed molecules is kinetically favored, leading initially to the formation of long and slightly branched chains and subsequently to intra-molecular condensations and cyclization [16,45,46]. The successive condensations form the polymeric network and the first colloidal particles (φ = 10–100 nm), which give rise to a spontaneous and ho-

mogeneous nucleation process when their critical radius is reached. It should be noted that gelation of the hybrid material is slower because triethoxysilanes have only three potential directions of polymerization. Unlike in the hydrolysis process, where the more the substituent of the precursor is withdrawn, the more favored is the condensation, because it favors nucleophilic attack on the silicon atom of a neighboring molecule. In this way, the condensation rate increases in the order MTEOS > ETEOS > PTEOS for the alkyl series and ClMTEOS > ClETEOS > ClPTEOS for the chloroalkyl series. In addition, chloroalkyl groups restrict the crosslinking between oligomers due to electrostatic repulsions, which destabilize the colloids and prevent the gelling process above a given molar percentage. Thus, it was possible to synthesize hybrid xerogels with molar percentages of up to 35%, 25% and 25% for the chloroalkyl series (ClMTEOS, ClETEOS and ClPTEOS respectively, Figure S1), while the molar percentages were substantially higher for the alkyl series [36–38].

Hence, with regard to the gelation times of the synthesized materials, there is a balance between the inductive/steric effects of the organic substituents of the precursor and the electrostatic effect between colloids. This electrostatic effect was a determining factor in the gelation times of chloroalkyl xerogels with a high percentage of precursor, due to the chlorine atom. The corresponding data are displayed in Figure 1a, which depicts the variation in gelation times of the chloroalkyl xerogels as a function of the molar percentage of precursor. It should be noted that gelation times for percentages higher than 10% have been omitted for the ClPTEOS series because they do not follow the trend observed for 0 to 10 molar percentages due to the limitations imposed by steric and electrostatic factors. In all cases, an increase in the molar percentage lengthens the gelation time, and this trend is also observed in xerogels prepared with analogous alkyl precursors, as shown in Figure 1b [36–38]. Figure 1c compares gelation times between the chloroalkyl xerogels and their non-chlorinated analogs, showing that the effect of the chlorine atom is more pronounced in the ClETEOS and ClPTEOS series, besides being opposite to the effect in the ClMTEOS series. This is because the alkyl chain is longer in the ClETEOS and ClPTEOS, increasing the steric effect and the repulsions between colloids created by the chlorine atom, which markedly lengthens the gelation time in comparison to their analogous non-chlorinated series. The chain is shorter in the ClMTEOS series; therefore, the steric effect is less pronounced and the repulsion between colloids is lower, favoring crosslinking in comparison to the longer chain chloroalkyl series. Furthermore, the withdrawing effect of the chlorine atom on the adjacent silicon atom is maximized, favoring condensation. Accordingly, the gelation times for the ClMTEOS series are reduced with respect to the analogous non-chlorinated series.

It should be noted that t_g values are higher for the ClETEOS series than for the other two chloroalkyl series and fit a linear rather than exponential trend (Figure 1a). This is because the length of the chloroethyl chain is not as short as in the ClMTEOS series or as long as in the ClPTEOS series, which has greater flexibility and freedom of movement. As demonstrated below, the behavior of this substituent is different because its size and nature necessarily place it in the network at fixed positions, minimizing repulsions. The lack of freedom of movement hinders and slows crosslinking, markedly increasing gelation times and forming periodic structures that create ordered domains in the silica network, as explained below.

3.2. Study of the Local Structure of Hybrid Xerogels Using FTIR and XRD

Figure 2 depicts, as an example, the FTIR spectra of the three chloroalkyl series with 20% molar percentage of the precursor in two wavelength ranges: (i) 4000–2750 cm^{-1} and (ii) 1600–400 cm^{-1}. The spectra obtained for the xerogels prepared with different molar percentages of chloroalkyl precursor and the different modes of vibration are reported in Supplementary Material with corresponding citations from the literature (Figure S2, Table S1).
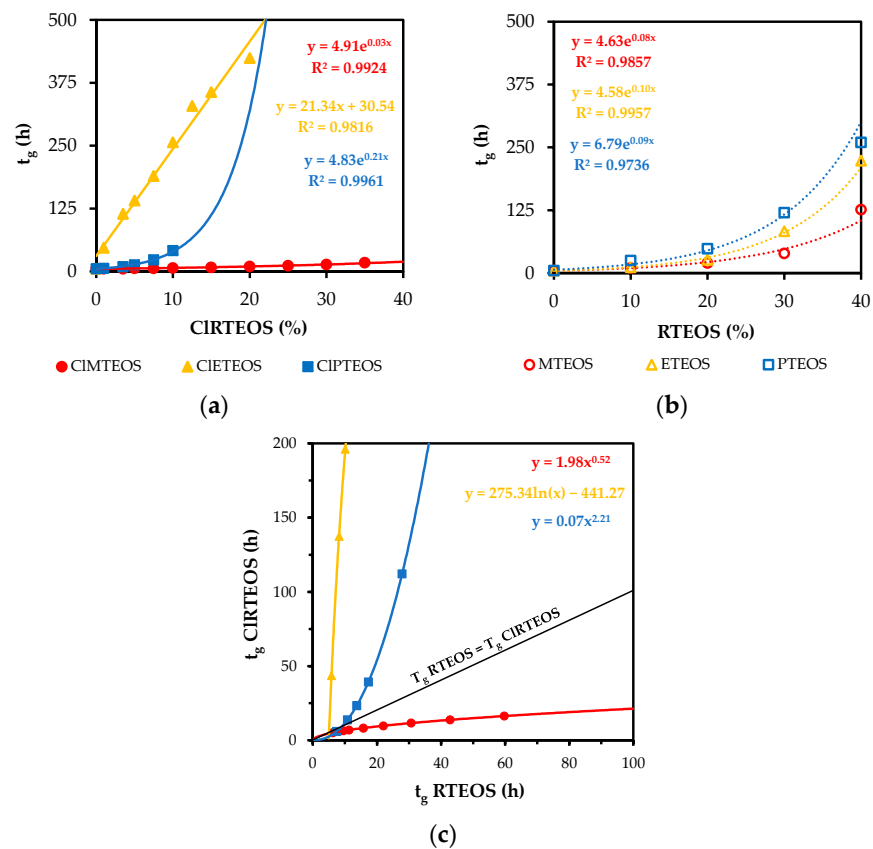
Figure 1. (**a**) t_g as a function of the percentage of precursor in the TEOS:ClRTEOS series, (**b**) t_g as a function of the percentage of t precursor in the TEOS:RTEOS series, and (**c**) t_g of the ClRTEOS versus RTEOS series.
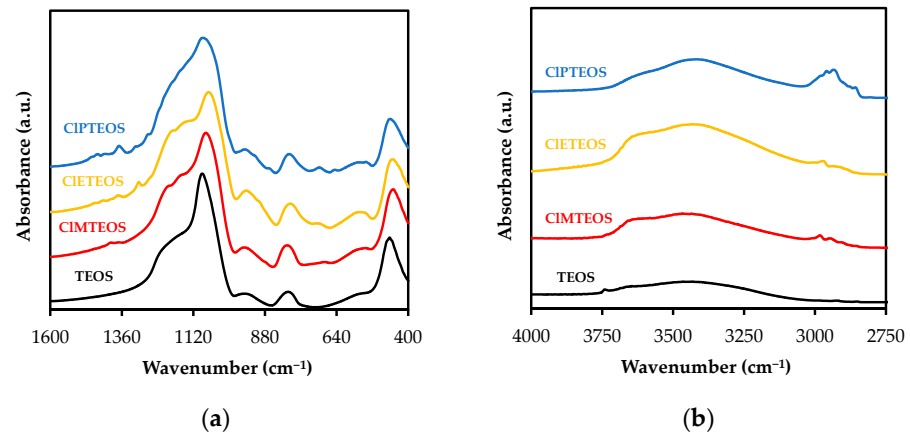

Figure 2. FTIR spectra of TEOS xerogel and TEOS:ClRTEOS hybrids (molar ratio, 20%): (**a**) range from 1600 to 400 cm^{-1}, and (**b**) range from 4000 to 2750 cm^{-1}.

Figure 2a depicts the characteristic FTIR bands of the silica lattice: (i) rocking of O-Si-O (ρ O-Si-O) at 455 cm^{-1}, (ii) symmetric stretching vibration of Si-O-Si (ν_s Si-O-Si) at 800 cm^{-1}, (iii) stretching of the Si-O bond belonging to surface silanes (ν_s Si-OH) at 955 cm^{-1}, (iv) asymmetric stretching vibration Si-O-Si at 1090 cm^{-1} (ν_{as} Si-O-Si), and (v) a broad and intense shoulder at 1200 cm^{-1} related to various modes of vibration of the Si-O-Si bonds [47]. Additionally, materials synthesized using silsesquioxanes typically show a set of Si-O-Si vibrations belonging to different structures: (i) bicyclic species at 1007 cm^{-1}, (ii) linear species at 1020 cm^{-1}, and (iii) cyclic species at 1050 cm^{-1} [48]. As can be observed in the figure, bands associated with bicyclic and linear species do not appear

to overlap with the band at 1090 cm^{-1}, indicating that these structures are present in lower proportions than are the cyclic structures. Figure 2b displays the bands of isolated (or non-interacting) surface silanols and silanols interacting by hydrogen bonds at 3660 cm^{-1} and 3450 cm^{-1}, respectively. These bands, which are also characteristic of silicon xerogels, indicate the hydrophobic or hydrophilic nature of the material [49]. In addition to the aforementioned bands, a shoulder is observed at 550 cm^{-1} in all spectra, associated with the presence of 4-membered siloxane rings, $(SiO)_4$ [50,51], which is consistent with the aforementioned assumption of the predominance of cyclic species.

The presence of organic groups in these hybrid materials is revealed by the bond vibrations of the alkyl chain: (i) C-H, (ii) C-C; and (iii) C-Cl. In Figure 2b, the characteristic bands of symmetric and asymmetric stretching of C-H are clearly observed between 2890 and 2975 cm^{-1}, showing an increase in intensity with longer chain length from being practically null in TEOS to being readily identifiable in ClPTEOS. The same can be seen in Figure 2a for the region between 1250 and 1400 cm^{-1}, which shows the bands of deformation modes related to C-H bonds (δ C-H) [52]. The symmetric stretching band C-C (ν_s C-C) of chloroethyl was detected in ClETEOS series at 900 cm^{-1} [53], while two well-differentiated bands were detected at 920 and 870 cm^{-1} in the ClPTEOS series, corresponding to the C-C bond contiguous to the chlorine and silicon atom, respectively (Table S1). This figure also depicts C-Cl stretching vibration bands (ν C-Cl) in the region between 750 and 650 cm^{-1} [53,54], with an increased intensity at higher molar percentages of ClRTEOS, as expected (Figure S2). It should be noted that it was not possible to detect the spectral band of the wagging vibration of the Si-CH$_2$ bond (ω C-H) in the region between 1300 and 980 cm^{-1} and the band corresponding to the out-of-plane deformation of the Si-C bond due to overlap with the frequencies of the bending vibration of the Si-O bond at 800 cm^{-1}. However, both vibrations can be clearly observed in the attenuated total reflection (ATR) spectrum of the pure precursor (Figure S3).

In the alkyl series previously studied by our research group (RTEOS:TEOS, R = M, E or P), a splitting of the band is observed at high percentages of alkyl precursor, moving the original band to lower frequency values due to the inductive effect of alkyl groups [36–38]. In the ETEOS series, for example, the band at 1092 cm^{-1} shifts to 1043 cm^{-1} and a new band appears at 1128 cm^{-1}, increasing its relative absorbance with higher molar percentage of ETEOS. The appearance of this band is related to the presence of highly symmetric structures within the amorphous silica matrix (Figure 3). These structures comprise four-membered silicon rings $(SiO)_4$ and are described as close or open cages (T_8 and T_7, respectively) and short ladders [54,55]. The intensity of this new band increases with higher molar percentage of the chloroalkyl precursor due to stabilization of the rings $(SiO)_4$ and minimization of the electrostatic repulsions produced by the chlorine atoms. In the chloroalkyl series, the asymmetric Si-O-Si vibration also shifts towards lower frequency values with increased proportion of the precursor. The bands are not resolved in this case because the molar percentage reached is lower than in the alkyl series; instead, shoulders are observed at around 1200 cm^{-1}.
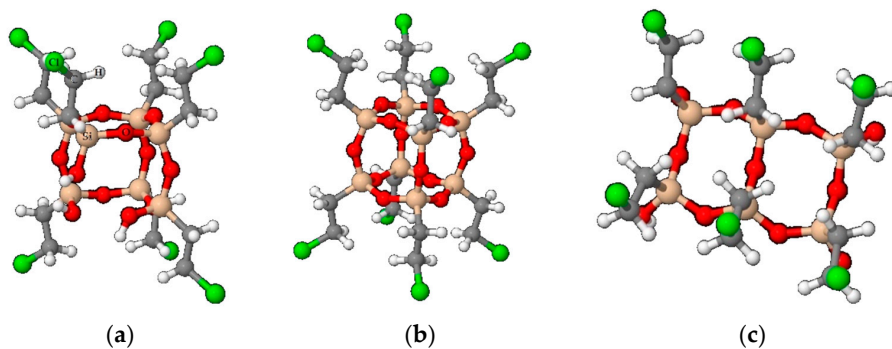

| (a) | (b) | (c) |

Figure 3. Ordered structures in the silica matrix built by $(SiO)_4$ rings in ClETEOS as an example: (**a**) open cage (T_7), (**b**) cage (T_8), and (**c**) short ladders.

The presence of these structures in both RTEOS:TEOS and ClRTEOS:TEOS hybrid xerogels is consistent with the X-ray diffraction spectra obtained for these materials. Figure 4 depicts the X-ray diffraction spectra of the ClETEOS:TEOS series (the only series that follows a linear trend in gelation times). In addition to the characteristic diffraction peak of amorphous silica (2θ ~ 24) [56,57], another peak can be observed at 2θ < 10° with only 1% of precursor. This peak is related to cage-like and ladder-like oligomeric species that form ordered domains within the amorphous matrix of the xerogel [58,59], which, according to computational chemistry studies, are the most thermodynamically stable structures for MTEOS:TEOS hybrid xerogels at pH 4.5 [60]. In the analogous ETEOS series, this diffraction peak is detected above 30% ETEOS and is consistent with the mass spectrometry results, which indicate the presence of ladder-like structures within the silica matrix [37]. Consequently, the appearance of this peak at much lower molar percentages in the ClETEOS series can be explained by the steric and electronic properties of the chloroethyl substituent, conferring rigidity or freedom of movement restriction to the organic moiety. This compromises the crosslinking and encourages the early formation of ordered periodic domains in the 3D structure. The difficult cross-linking of the colloids or oligomers would explain the anomalous trends in gelation times for this series. The spectra of the series of hybrid xerogels and the corresponding data are exhibited in Supplementary Material (Figure S4, Table S2).
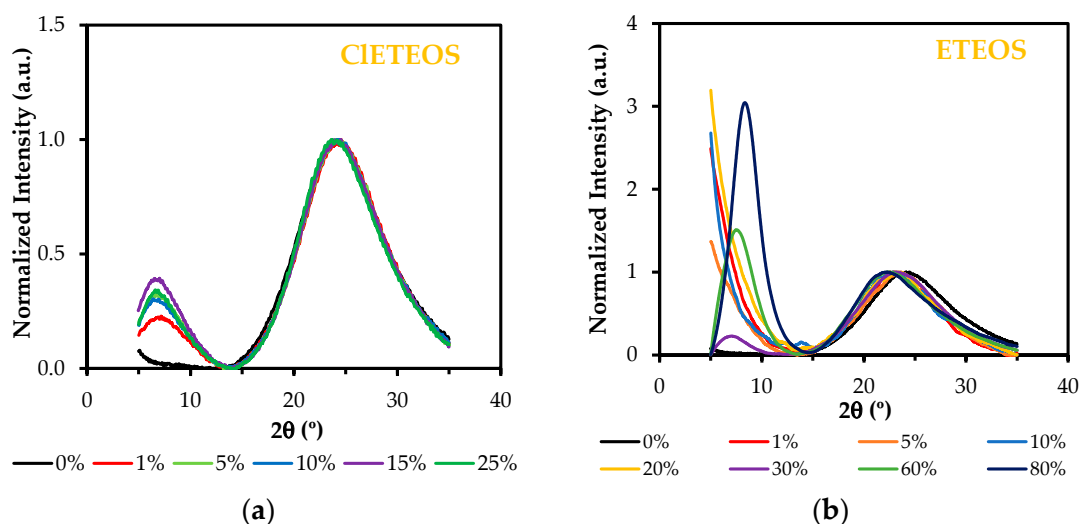

Figure 4. X-ray diffraction spectra of the hybrid xerogels at different molar percentages (normalized with respect to the band 2θ ~4°: (**a**) ClETEOS:TEOS, and (**b**) ETEOS:TEOS.

3.3. Spectral Deconvolution of the 1300–700 cm^{-1} Region

Figure 5 depicts the ν_{as} Si-O-Si band at 1090 cm^{-1} and the associated shoulder at around 1200 cm^{-1}. It shows the shift at lower frequencies of the band at 1090 cm^{-1} with higher molar percentages of the precursor as well as the overlapping bands derived from the shoulder at 1200 cm^{-1}. These emerging bands are attributable to the different structures that make up the siloxane bonds, mostly forming rings of four or six silicon atoms, $(SiO)_4$ and $(SiO)_6$ respectively. The relative abundance of these rings depends on the nature and molar ratio of the precursor: four-fold rings are the predominant species in xerogels and are thermodynamically favored in the oligomerization of TEOS at acid pH through cyclodimerization processes [45,47], whereas six-fold rings are kinetically favored over four-membered rings and constitute the main structures of silicates and amorphous silica [17,61,62]. In the deconvolution study, each structure is associated with two optical modes of ν_{as} Si-O-Si vibration in the FTIR spectra due to the Coulomb interactions: (i) transverse mode (TO), between 1100 and 1000 cm^{-1}; and (ii) longitudinal mode (LO), between 1250 and 1100 cm^{-1} [63].
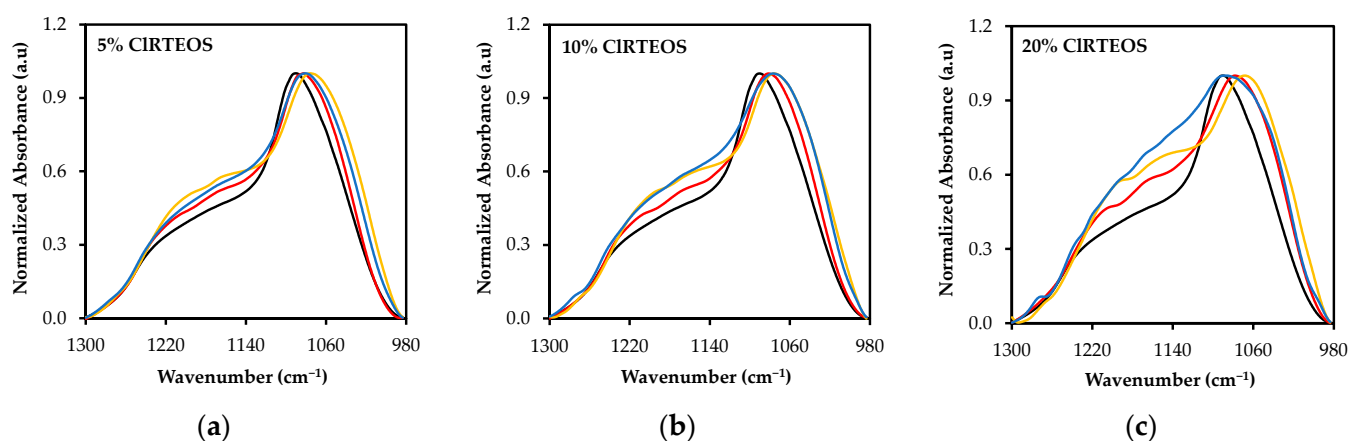
Figure 5. Normalized FTIR spectra of the 1300–980 cm^{-1} region of the TEOS xerogel (black), and those of the three chloroalkyl series at different molar ratios: (**a**) 5%, (**b**) 10%, and (**c**) 20%. (ClMTEOS (red), ClETEOS (yellow), and ClPTEOS (blue)).

The changes in these structures as the precursor increases and their relative proportions were studied by deconvolution of the FTIR spectra in the range 1300–980 cm^{-1}, using the non-linear least-squares method to obtain the Gaussian-Lorentzian components. The different distances and degrees of torsion of Si-O-Si bonds in the structures, along with the optical modes, predict four components of ν_{as} Si-O-Si in the studied range: (i) TO$_4$ and LO$_4$ for (SiO)$_4$ rings, and (ii) TO$_6$ and LO$_6$ for (SiO)$_6$ rings. Therefore, four components were introduced in the software for deconvolution of the reference material spectrum (100% TEOS Xerogel, Figure 2). The resulting optimized synthetic spectrum was composed of bells with maxima at 1214, 1143, 1092 and 1078 cm^{-1}, assigned to LO6, LO$_4$, TO$_4$ and TO$_6$, respectively. This assignation takes account of: (i) the aforementioned frequency ranges of the optical modes; (ii) the predominance of (SiO)$_4$ species evidenced by the shoulder at 550 cm^{-1} in the spectra, and (iii) the broader limiting frequencies in both optical modes for six-fold rings, related to their less tensioned nature (Figure 6) [27,47,64].
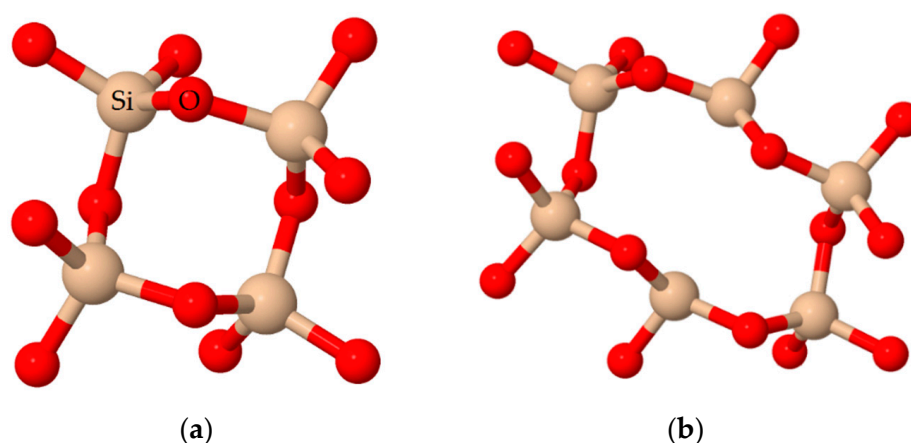

Figure 6. Predominant structures within the silica matrix of a xerogel prepared with TEOS: (**a**) (SiO)$_4$ rings, and (**b**) (SiO)$_6$ rings.

Spectra of the RTEOS:TEOS and ClRTEOS:TEOS series were deconvoluted using the aforementioned frequencies obtained from the reference material (LO$_6$, LO$_4$, TO$_4$ and TO$_6$) and the frequencies of C-H wagging vibrations corresponding to the organic moiety of each precursor (Table S1, supporting material). By way of example, Figure 7 depicts the synthetic spectra derived from the bell-shaped curves obtained for TEOS (Figure 7a) and the organochlorinated xerogels with a 20% molar percentage of precursor (actual FTIR spectra shown in Figure 5c).
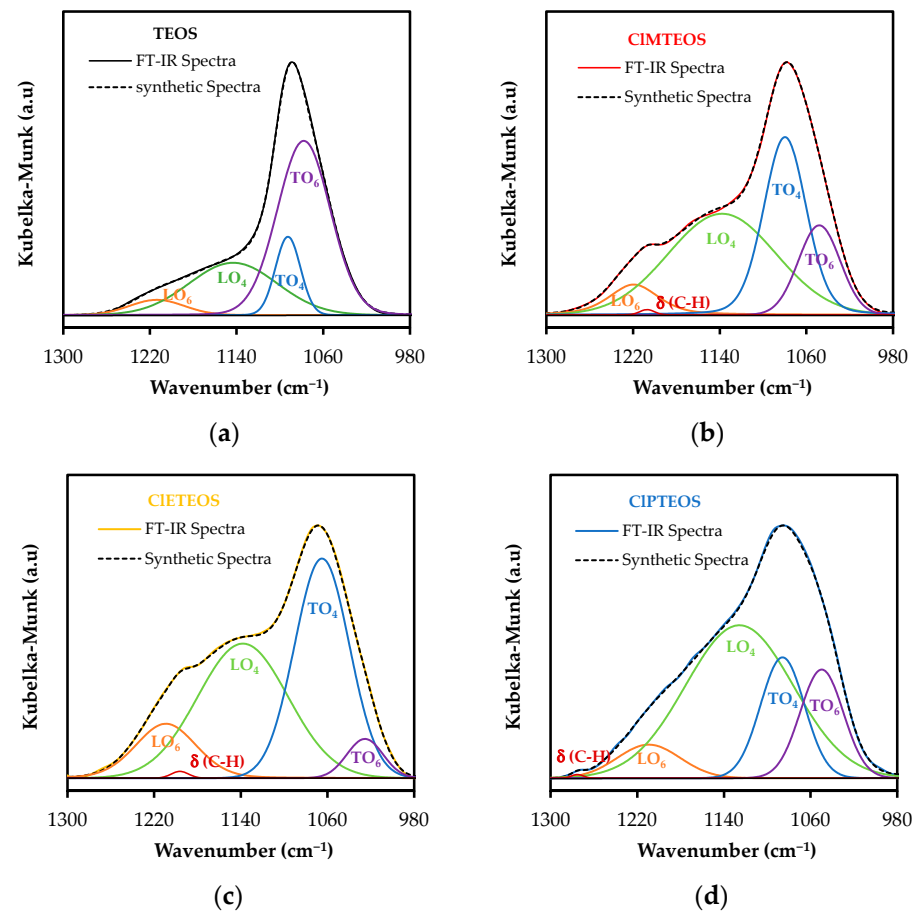
Figure 7. Deconvolution and least-squares adjustment of the FTIR spectra of the xerogels: (**a**) Reference material (100% TEOS), (**b**) 20% ClMTEOS, (**c**) 20% ClETEOS, and (**d**) 20% ClPTEOS.

Based on the integrated areas of the Gaussian-Lorentzian bells, Equations (6) and (7) were calculated to determine the relative abundance of $(SiO)_6$ and $(SiO)_4$ rings (Tables S3 and S4 for the ClRTEOS:TEOS and RTEOS:TEOS series, respectively).

$$(SiO)_6, \% = \frac{A(LO_6) + A(TO_6)}{A(LO_4) + A(TO_4) + A(LO_6) + A(TO_6)} \; 100, \tag{6}$$

$$(SiO)_4, \% = \frac{A(LO_4) + A(TO_4)}{A(LO_4) + A(TO_4) + A(LO_6) + A(TO_6)} \; 100, \tag{7}$$

where $A(LO_6)$ is the area of the band at 1220 cm^{-1}, $A(LO_4)$ is the area of the band at 1150 cm^{-1}; $A(TO_4)$ is the area of the band at 1070 cm^{-1} and $A(TO_6)$ the area of the band at 1050 cm^{-1}.

Figure 8 graphically depicts the $(SiO)_4/(SiO)_6$ ratio as a function of the molar percentage of chloroalkyl precursor (data obtained from Tables S3 and S4, see Supplementary Material). It shows that the formation of $(SiO)_4$ rings is more favored with longer chloroalkyl chain for a given molar percentage of precursor. The $(SiO)_4/(SiO)_6$ ratio increases exponentially with a higher percentage of precursor in the three series. These trends are not expected, because the entry of organic molecules or substituents into the network should produce an increase in the proportion of $(SiO)_6$ species, which minimizes steric tension, increases the volume, and markedly reduces the density (Table S5). Accordingly, Fidalgo, A. et al. found that the proportion of $(SiO)_6$ rings increases with higher molar percentage of RTEOS (R = M, E and P), reaching an abundance of almost 85% for samples with a precursor percentage of 75% [27]. However, the synthesis of these materials was performed in basic medium, explaining the greater abundance of six-membered rings

from crosslinking between more branched chains. In the case of the present xerogels, the higher proportion of $(SiO)_4$ rings in the chloroalkyl series would be related not only to their synthesis in acidic medium but also to the formation of ordered domains at very low molar percentages of precursor. The data in Table S3 (Supplementary Material) for the three chloroalkyl series show that the contribution of the LO_4 band (attributable to the total percentage of $(SiO)_4$ rings) increases with higher percentage of precursor. This is a relevant finding, given that this band is also associated with the presence of ordered structures in the literature [5,51,65]. Its presence is closely related to a decrease in the degree of crosslinking in the xerogel, in agreement with the shifts at lower wavelengths of the TO_4 band, which is associated with the silicon network [13]. Another factor that supports the formation of these ordered structures is the decrease in the intensity of the LO_6 band (see Table S3), because this bands is generally associated not only with $(SiO)_6$ rings but also with the non-silica porous skeleton [66].
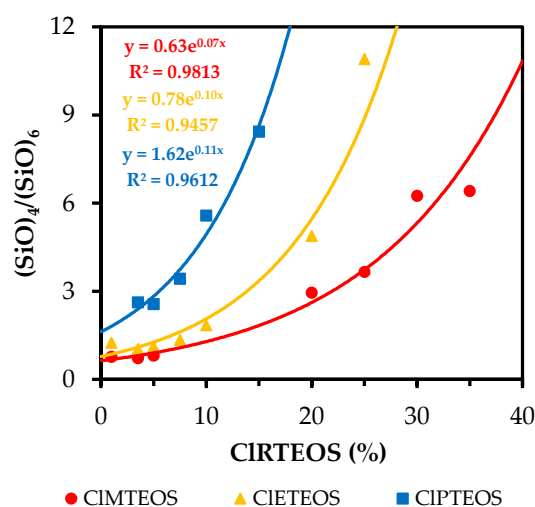

Figure 8. Variation in $(SiO)_4/(SiO)_6$ as a function of the molar percentage of precursor in ClR-TEOS:TEOS xerogels.

The way in which the chlorine atom affects the ring distribution was studied in greater depth by performing interpolations using the equations of the exponential curves shown in Figure 8 and Figure S5 ($(SiO)_4/(SiO)_6$ vs. %RTEOS). These equations were used to obtain $(SiO)_4/(SiO)_6$ ratios for percentages of the precursor in the range 1–35% in both the chlorinated series and their non-chlorinated analogs (the data used are exhibited in Table S6 of Supplementary Material).

Figure 9 compares $(SiO)_4/(SiO)_6$ ratios between the ClRTEOS:TEOS series and the RTEOS:TEOS series to show how the chlorine atom affects the relative proportion of species.

A discontinuous black straight line has been added in this figure to depict the hypothetical case in which the ratio of $(SiO)_4/(SiO)_6$ rings is the same for the alkyl and chloroalkyl series at the same molar percentage of precursor, which would indicate that the chlorine atom in the ClRTEOS precursor has no effect on the $(SiO)_4$:$(SiO)_6$ ratio with respect to its counterpart, RTEOS. Above this line, the effect of the chlorine on the $(SiO)_4$:$(SiO)_6$ ratio is positive, favoring the formation of $(SiO)_4$ rings. Below this line, the effect of the chlorine is negative, favoring the formation of $(SiO)_6$ structures. The figure shows that this ratio is lower in the ClMTEOS than in the MTEOS series. This trend is consistent with the behavior observed in Figure 1c, which shows that the ClMTEOS series has shorter gelation times, closely related to the size of the chloroalkyl chain. This not only fails to produce a significant steric or electrostatic effect to disfavor the formation of $(SiO)_6$ rings (kinetically favored species), but also accelerates condensation due to the inductive effect of the chlorine, which reduces gelation times and gives rise to lower $(SiO)_4/(SiO)_6$ ratios. Unlike the ClMTEOS series, the $(SiO)_4/(SiO)_6$ values for the ClETEOS and ClPTEOS series are higher than those of their analogs throughout the region, which is in turn consistent

with the longer gelation times displayed in Figure 1c. In these two series, the steric factor and the electrostatic repulsions between colloids significantly increase the crosslinking time, disfavoring $(SiO)_6$ ring formation. The slope of these curves is much steeper than the slope observed for ClMTEOS series, implying that the addition of a higher percentage of precursor increases the influence exerted by the chlorine atom on the structure of the synthesized materials, which is maximized in ClPTEOS:TEOS, the series with the longest chain. It should be noted that, although the $(SiO)_4/(SiO)_6$ ratio is slightly lower in the ClETEOS versus ClPTEOS series, the former has longer gelation times and peaks at small angles ($10° < 2\theta$) in all X-ray diffraction spectra. According to these findings, the chloroethyl moiety in this material is more efficient in directing the formation of ordered domains and nanostructuring the material, even when it has fewer $(SiO)_4$ rings (related to periodic box or ladder-type structures), consistent with the results of all techniques used to characterize these hybrid materials [35].
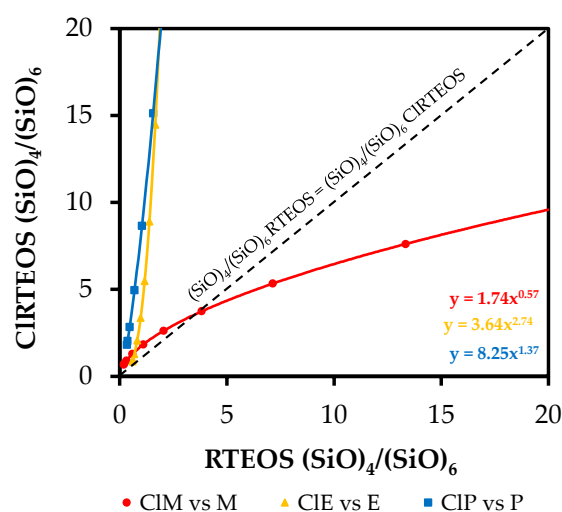

Figure 9. Variation in the proportion of structures $(SiO)_4/(SiO)_6$ of the chloroalkyl series with respect to the alkyl series at different molar percentages of precursor.

4. Conclusions

In general, an increase in the molar percentage of the precursor (ClRTEOS and RTEOS) translates into an increase in gelation times due to conjugation of the steric and inductive effects of the organic substituents. The gelation times of the chloroalkyl series are longer than those of their analogous alkyl series for long alkyl chains (ClETEOS and ClPTEOS), although they are slightly shorter for the shortest alkyl chain (ClMTEOS). This is explained by the maximization of the inductive effect of the chlorine atom due to its proximity to the silicon atom, which exerts a positive influence on the condensation and crosslinking reactions, the slowest step in the sol-gel process. On the other hand, a larger number of carbons in the alkyl chain reduces the inductive effect of the chlorine on the silicon atom and increases the steric effect exerted by the chain to form the silica network; this effect is maximized in the series bearing ethyl, chloroethyl, propyl and chloropropyl groups. Unexpectedly, the ClETEOS series have the highest gelation times, explained by: (i) the lack of flexibility of the chloroethyl group due to the steric tension caused by its size; (ii) the electrostatic repulsions exerted by chlorine, forcing the formation of kinetically disfavored structures in order to minimize its energy; and (iii) the X-ray diffraction spectra of this series (1–25%), which reveal maximum diffraction at a small angle ($2\theta < 10°$), consistent with the presence in their structure of periodic domains that require more time for their formation. The FTIR spectra of each hybrid xerogel yielded data for a semi-quantitative determination of the proportions of $(SiO)_4$ and $(SiO)_6$ rings by deconvolution methods. These findings reveal a competitive process between the two species that is dependent on the precursor and its molar ratio, observing similar trends to those obtained for the gelation times. In the ClMTEOS series, the presence of the chlorine atom favors the formation of

six-fold rings. An opposite trend is observed in the ClETEOS and ClPTEOS series, favoring the formation of 4-fold rings; in addition, the chlorine atom exerts a stronger influence in the ClETEOS and ClPTEOS series, consistent with their longer gelation times and the presence of periodic structures. According to these results, the substitution of a hydrogen atom by a halogen functional group (e.g., chlorine) in hybrid xerogels produces relevant changes in its microstructure due to the intermolecular forces generated by the chlorine atom in the sol-gel process.

Supplementary Materials: The following are available online at https://www.mdpi.com/article/10.3390/polym13132082/s1, Figure S1: Images of the synthesized xerogels in which a change in morphology is observed with an increasing percentage of organic precursors: (**a**) TEOS, (**b**–**d**) ClMTEOS, (**e**–**g**) ClETEOS, and (**h**–**j**) ClPTEOS; Figure S2: FTIR spectra of the ClRTEOS:TEOS xerogels in the ranges 4000–2750 and 1600–400 cm^{-1}: (**a**,**b**) ClMTEOS, (**c**,**d**) ClETEOS, and (**e**,**f**) ClPTEOS; Figure S3: FTIR spectra of the precursors (TEOS, ClMTEOS, ClETEOS and ClPTEOS) in the ranges: (**a**) 4000–2750 cm^{-1} and (**b**) 1600–400 cm^{-1}; Figure S4: X-ray diffraction spectra of ClRTEOS:TEOS and RTEOS:TEOS xerogels: (**a**) ClMTEOS, (**b**) MTEOS, (**c**) ClPTEOS, and (**d**) PTEOS; Figure S5: $(SiO)_4/(SiO)_6$ ratio with respect to the molar percentage of RTEOS:TEOS xerogels. Table S1: FTIR spectra band assignment; Table S2: Bragg angles (2θ), band area (A), and bond distance (d1 and d2 (nm)) calculated from the X-ray diffraction peaks for the xerogels synthesized with ClMTEOS, MTEOS, ClPTEOS, and PTEOS; Table S3: Relative areas obtained from deconvolution of the FTIR spectra and percentages of $(SiO)_4$ and $(SiO)_6$ in the ClRTEOS:TEOS series; Table S4: Relative areas obtained from deconvolution of the FTIR spectra and percentages of $(SiO)_4$ and $(SiO)_6$ in the RTEOS:TEOS series; Table S5: Helium density of the hybrid xerogels; Table S6: experimental data of $(SiO)_4/(SiO)_6$ and equations used for Figure 8 and Table 1.

Author Contributions: G.C.-Q.: investigation, writing–original draft. M.E.-V.: methodology, resources, writing, review and editing. M.V.L.-R. writing–review and editing. J.J.G.: conceptualization, supervision, project administration, funding acquisition, writing, review and editing. All authors have read and agreed to the published version of the manuscript.

Data Availability Statement: The data presented in this study are available on request from the corresponding author.

Conflicts of Interest: The authors declare no conflict of interest.

References

1. Pastore, A.; Badocco, D.; Pastore, P. Influence of surfactant chain length, counterion and OrMoSil precursors on reversibility and working interval of pH colorimetric sensors. *Talanta* **2020**, *212*, 120739. [CrossRef]
2. Gillanders, R.N.; Campbell, I.A.; Glackin, J.M.E.; Samuel, I.D.W.; Turnbull, G.A. Ormosil-coated conjugated polymers for the detection of explosives in aqueous environments. *Talanta* **2018**, *179*, 426–429. [CrossRef]
3. Li, Z.; Suslick, K.S. Ultrasonic Preparation of Porous Silica-Dye Microspheres: Sensors for Quantification of Urinary Trimethylamine N-Oxide. *ACS Appl. Mater. Interfaces* **2018**, *10*, 15820–15828. [CrossRef]
4. Shamir, D.; Elias, I.; Albo, Y.; Meyerstein, D.; Burg, A. ORMOSIL-entrapped copper complex as electrocatalyst for the heterogeneous de-chlorination of alkyl halides. *Inorg. Chim. Acta* **2020**, *500*, 119225. [CrossRef]
5. Ponamoreva, O.N.; Afonina, E.L.; Kamanina, O.A.; Lavrova, D.G.; Arlyapov, V.A.; Alferov, V.A.; Boronin, A.M. Yeast Debaryomyces hansenii within ORMOSIL Shells as a Heterogeneous Biocatalyst. *Appl. Biochem. Microbiol.* **2018**, *54*, 736–742. [CrossRef]
6. Lin, W.; Zhang, X.; Cai, Q.; Yang, W.; Chen, H. Dehydrogenation-driven assembly of transparent and durable superhydrophobic ORMOSIL coatings on cellulose-based substrates. *Cellulose* **2020**, *27*, 7805–7821. [CrossRef]
7. Liu, Z.; Tian, S.; Li, Q.; Wang, J.; Pu, J.; Wang, G.; Zhao, W.; Feng, F.; Qin, J.; Ren, L. Integrated Dual-Functional ORMOSIL Coatings with AgNPs@rGO Nanocomposite for Corrosion Resistance and Antifouling Applications. *ACS Sustain. Chem. Eng.* **2020**, *8*, 6786–6797. [CrossRef]

8.   Scotland, K.M.; Shetranjiwalla, S.; Vreugdenhil, A.J. Curable hybrid materials for corrosion protection of steel: Development and application of UV-cured 3-methacryloxypropyltrimethoxysilane-derived coating. *J. Coat. Technol. Res.* **2020**, *17*, 977–989. [CrossRef]

9.   Bouvet-Marchand, A.; Graillot, A.; Abel, M.; Koudia, M.; Boutevin, G.; Loubat, C.; Grosso, D. Distribution of fluoroalkylsilanes in hydrophobic hybrid sol-gel coatings obtained by co-condensation. *J. Mater. Chem. A* **2018**, *6*, 24899–24910. [CrossRef]

10.   Yue, D.; Feng, Q.; Huang, X.; Zhang, X.; Chen, H. In situ fabrication of a superhydrophobic ORMOSIL coating on wood by an ammonia-HMDS vapor treatment. *Coatings* **2019**, *9*, 556. [CrossRef]

11.   Malek, S.K.; Nodeh, H.R.; Akbari-Adergani, B. Silica-based magnetic hybrid nanocomposite for the extraction and preconcentration of some organophosphorus pesticides before gas chromatography. *J. Sep. Sci.* **2018**, *41*, 2934–2941. [CrossRef] [PubMed]

12.   Moriones, P.; Ríos, X.; Echeverría, J.C.; Garrido, J.J.; Pires, J.; Pinto, M. Hybrid organic-inorganic phenyl stationary phases for the gas separation of organic binary mixtures. *Colloids Surf. A Physicochem. Eng. Asp.* **2011**, *389*, 69–75. [CrossRef]

13.   Tran, H.N.; Nghiem, T.H.L.; Vu, D.T.T.; Pham, M.T.; Nguyen, T.V.; Tran, T.T.; Chu, V.H.; Tong, K.T.; Tran, T.T.; Le, X.T.T.; et al. Dye-doped silica-based nanoparticles for bioapplications. *Adv. Nat. Sci. Nanosci. Nanotechnol.* **2013**, *4*, 043001. [CrossRef]

14.   Judeinstein, P.; Sanchez, C. Hybrid organic-inorganic materials: A land of multidisciplinarity. *J. Mater. Chem.* **1996**, *6*, 511–525. [CrossRef]

15.   Alemán, J.; Chadwick, A.V.; He, J.; Hess, M.; Horie, K.; Jones, R.G.; Kratochvíl, P.; Meisel, I.; Mita, I.; Moad, G.; et al. Definitions of terms relating to the structure and processing of sols, gels, networks, and inorganic-organic hybrid materials (IUPAC recommendations 2007). *Pure Appl. Chem.* **2007**, *79*, 1801–1829. [CrossRef]

16.   Brinker, C.J.; Scherer, G.W. *Sol-Gel Science*; Academic Press: New York, NY, USA, 1990; ISBN 978-0-08-057103-4.

17.   Fidalgo, A.; Ilharco, L.M. The defect structure of sol-gel-derived silica/polytetrahydrofuran hybrid films by FTIR. *J. Non Cryst. Solids* **2001**, *283*, 144–154. [CrossRef]

18.   Chemtob, A.; Ni, L.; Croutxé-Barghorn, C.; Boury, B. Ordered hybrids from template-free organosilane self-assembly. *Chem. A Eur. J.* **2014**, *20*, 1790–1806. [CrossRef] [PubMed]

19.   Issa, A.A.; Luyt, A.S. Kinetics of alkoxysilanes and organoalkoxysilanes polymerization: A review. *Polymers* **2019**, *11*, 537. [CrossRef] [PubMed]

20.   Cheng, X.; Chen, D.; Liu, Y. Mechanisms of silicon alkoxide hydrolysis-oligomerization reactions: A DFT investigation. *ChemPhysChem* **2012**, *13*, 2392–2404. [CrossRef]

21.   Issa, A.A.; El-Azazy, M.; Luyt, A.S. Kinetics of alkoxysilanes hydrolysis: An empirical approach. *Sci. Rep.* **2019**, *9*, 1–15. [CrossRef]

22.   Echeverría, J.C.; Moriones, P.; Arzamendi, G.; Garrido, J.J.; Gil, M.J.; Cornejo, A.; Martínez-Merino, V. Kinetics of the acid-catalyzed hydrolysis of tetraethoxysilane (TEOS) by 29Si NMR spectroscopy and mathematical modeling. *J. Sol-Gel Sci. Technol.* **2018**, *86*, 316–328. [CrossRef]

23.   Moriones, P.; Arzamendi, G.; Cornejo, A.; Garrido, J.J.; Echeverria, J.C. Comprehensive Kinetics of Hydrolysis of Organotriethoxysilanes by 29Si NMR. *J. Phys. Chem. A* **2019**, *123*, 10364–10371. [CrossRef]

24.   Colin, B.; Lavastre, O.; Fouquay, S.; Michaud, G.; Simon, F.; Laferte, O.; Brusson, J.-M. Contactless Raman Spectroscopy-Based Monitoring of Physical States of Silyl-Modified Polymers during Cross-Linking. *Green Sustain. Chem.* **2016**, *6*, 151–166. [CrossRef]

25.   Innocenzi, P.; Falcaro, P.; Grosso, D.; Babonneau, F. Microstructural evolution and order-disorder transitions in mesoporous silica films studied by FTIR spectroscopy. *Mater. Res. Soc. Symp. Proc.* **2002**, *726*, 271–281. [CrossRef]

26.   Ponton, S.; Dhainaut, F.; Vergnes, H.; Samelor, D.; Sadowski, D.; Rouessac, V.; Lecoq, H.; Sauvage, T.; Caussat, B.; Vahlas, C. Investigation of the densification mechanisms and corrosion resistance of amorphous silica films. *J. Non Cryst. Solids* **2019**, *515*, 34–41. [CrossRef]

27.   Fidalgo, A.; Ciriminna, R.; Ilharco, L.M.; Pagliaro, M. Role of the alkyl-alkoxide precursor on the structure and catalytic properties of hybrid sol-gel catalysts. *Chem. Mater.* **2005**, *17*, 6686–6694. [CrossRef]

28.   Saputra, R.E.; Astuti, Y.; Darmawan, A. Hydrophobicity of silica thin films: The deconvolution and interpretation by Fourier-transform infrared spectroscopy. *Spectrochim. Acta Part A Mol. Biomol. Spectrosc.* **2018**, *199*, 12–20. [CrossRef]

29.   Stocker, M.K.; Sanson, M.L.; Bernardes, A.A.; Netto, A.M.; Brambilla, R. Acid–base sensor based on sol–gel encapsulation of bromothymol blue in silica: Application for milk spoilage detection. *J. Sol-Gel Sci. Technol.* **2021**, *98*, 568–579. [CrossRef]

30.   Fidalgo, A.; Ilharco, L.M. Correlation between physical properties and structure of silica xerogels. *J. Non Cryst. Solids* **2004**, *347*, 128–137. [CrossRef]

31.   Izaak, T.I.; Martynova, D.O.; Stonkus, O.A.; Slavinskaya, E.M.; Boronin, A.I. Deposition of silver nanoparticles into porous system of sol-gel silica monoliths and properties of silver/porous silica composites. *J. Sol-Gel Sci. Technol.* **2013**, *68*, 471–478. [CrossRef]

32.   Capeletti, L.B.; Zimnoch, J.H. Fourier Transform Infrared and Raman Characterization of Silica-Based Materials. In *Applications of Molecular Spectroscopy to Current Research in the Chemical and Biological Sciences*, 1st ed.; Stauffer, M., Ed.; Intechopen: Kansas City, KS, USA, 2016; pp. 3–22, ISBN 978-953-51-2681-2.

33.   Echeverría, J.C.; Faustini, M.; Garrido, J.J. Effects of the porous texture and surface chemistry of silica xerogels on the sensitivity of fiber-optic sensors toward VOCs. *Sens. Actuators B Chem.* **2016**, *222*, 1166–1174. [CrossRef]

34.   Echeverría, J.C.; Calleja, I.; Moriones, P.; Garrido, J.J. Fiber optic sensors based on hybrid phenyl-silica xerogel films to detect n-hexane: Determination of the isosteric enthalpy of adsorption. *Beilstein J. Nanotechnol.* **2017**, *8*, 475–484. [CrossRef] [PubMed]

35.   Cruz-Quesada, G.; Espinal-Viguri, M.; Garrido, J. Novel Organochlorinated Xerogels: From Microporous Materials to Ordered Domains. *Polymers* **2021**, *13*, 1415. [CrossRef]

36. Rios, X.; Moriones, P.; Echeverría, J.C.; Luquín, A.; Laguna, M.; Garrido, J.J. Characterisation of hybrid xerogels synthesised in acid media using methyltriethoxysilane (MTEOS) and tetraethoxysilane (TEOS) as precursors. *Adsorption* **2011**, *17*, 583–593. [CrossRef]
37. Rios, X.; Moriones, P.; Echeverría, J.C.; Luquin, A.; Laguna, M.; Garrido, J.J. Ethyl group as matrix modifier and inducer of ordered domains in hybrid xerogels synthesised in acidic media using ethyltriethoxysilane (ETEOS) and tetraethoxysilane (TEOS) as precursors. *Mater. Chem. Phys.* **2013**, *141*, 166–174. [CrossRef]
38. Moriones, P. Sintesis y Caracterización de Xerogeles Silíceos Híbridos (RTEOS/TEOS.; R = P, Ph). Ph.D. Thesis, Universidad Publica de Navarra, Pamplona, Spain, 2015. Available online: https://academica-e.unavarra.es/handle/2454/20351 (accessed on 14 November 2020).
39. Torres-Luna, J.A.; Carriazo, J.G. Porous aluminosilicic solids obtained by thermal-acid modification of a commercial kaolinite-type natural clay. *Solid State Sci.* **2019**, *88*, 29–35. [CrossRef]
40. Sakka, S. Handbook of Sol-Gel Science and technology processing characterization and applications. In *Characterization of Sol-Gel materials and Products*; Kluwer Academic Publishers: Amsterdam, The Netherlands, 2005; Volume II, ISBN 1-4020-7967-2.
41. Berrier, E.; Courtheoux, L.; Bouazaoui, M.; Capoen, B.; Turrell, S. Correlation between gelation time, structure and texture of low-doped silica gels. *Phys. Chem. Chem. Phys.* **2010**, *12*, 14477–14484. [CrossRef]
42. Salon, B.M.C.; Belgacem, M.N. Competition between hydrolysis and condensation reactions of trialkoxysilanes, as a function of the amount of water and the nature of the organic group. *Colloids Surf. A Physicochem. Eng. Asp.* **2010**, *366*, 147–154. [CrossRef]
43. Pierre, A.C. *Introduction to Sol-Gel Processing*; Springer: Berlin/Heidelberg, Germany, 2020; ISBN 9780792381211.
44. Benbow, J.J. *Ultrastructure Processing of Advance Materials.*; Uhlmann, D.R., Ulrich, D.R., Eds.; John Wiley & Sons, INC.: New York, NY, USA, 1989; Volume 44, ISBN 0471529869.
45. Depla, A.; Verheyen, E.; Veyfeyken, A.; Van Houteghem, M.; Houthoofd, K.; Van Speybroeck, V.; Waroquier, M.; Kirschhock, C.E.A.; Martens, J.A. UV-Raman and 29Si NMR spectroscopy investigation of the nature of silicate oligomers formed by acid catalyzed hydrolysis and polycondensation of tetramethylorthosilicate. *J. Phys. Chem. C* **2011**, *115*, 11077–11088. [CrossRef]
46. Depla, A.; Lesthaeghe, D.; Van Erp, T.S.; Aerts, A.; Houthoofd, K.; Fan, F.; Li, C.; Van Speybroeck, V.; Waroquier, M.; Kirschhock, C.E.A.; et al. 29Si NMR and UV-raman investigation of initial oligomerization reaction pathways in acid-catalyzed silica Sol-Gel chemistry. *J. Phys. Chem. C* **2011**, *115*, 3562–3571. [CrossRef]
47. Fidalgo, A.; Ilharco, L.M. Chemical Tailoring of Porous Silica Xerogels: Local Structure by Vibrational Spectroscopy. *Chem. A Eur. J.* **2004**, *10*, 392–398. [CrossRef]
48. Hayami, R.; Ideno, Y.; Sato, Y.; Tsukagoshi, H.; Yamamoto, K.; Gunji, T. Soluble ethane-bridged silsesquioxane polymer by hydrolysis–condensation of bis(trimethoxysilyl)ethane: Characterization and mixing in organic polymers. *J. Polym. Res.* **2020**, *27*, 1–10. [CrossRef]
49. Ramezani, M.; Vaezi, M.R.; Kazemzadeh, A. The influence of the hydrophobic agent, catalyst, solvent and water content on the wetting properties of the silica films prepared by one-step sol-gel method. *Appl. Surf. Sci.* **2015**, *326*, 99–106. [CrossRef]
50. Innocenzi, P. Infrared spectroscopy of sol–gel derived silica-based films: A spectra-microstructure overview. *J. Non Cryst. Solids* **2003**, *316*, 309–319. [CrossRef]
51. Handke, M.; Kowalewska, A. Siloxane and silsesquioxane molecules—Precursors for silicate materials. *Spectrochim. Acta Part. A Mol. Biomol. Spectrosc.* **2011**, *79*, 749–757. [CrossRef]
52. Coates, J. Interpretation of Infrared Spectra, A Practical Approach. In *Encyclopedia of Analytical Chemistry*, 3rd ed.; Meyers, R.A., Ed.; Wiley & Sons, Ltd.: New York, NY, USA, 2006; pp. 1–23, ISBN 978-0-471-97670-7.
53. Launer, P.J.; Arkles, B. Infrared Analysis of Orgaonsilicon Compounds. In *Silicon Compounds: Silanes and Silicones*, 3rd ed.; Gelest Inc.: Morrisville, PA, USA, 2013; pp. 175–178.
54. Chen, G.; Zhou, Y.; Wang, X.; Li, J.; Xue, S.; Liu, Y.; Wang, Q.; Wang, J. Construction of porous cationic frameworks by crosslinking polyhedral oligomeric silsesquioxane units with N-heterocyclic linkers. *Sci. Rep.* **2015**, *5*, 1–14. [CrossRef]
55. Park, E.S.; Ro, H.W.; Nguyen, C.V.; Jaffe, R.L.; Yoon, D.Y. Infrared spectroscopy study of microstructures of poly(silsesquioxane)s. *Chem. Mater.* **2008**, *20*, 1548–1554. [CrossRef]
56. Kamiya, K.; Dohkai, T.; Wada, M.; Hashimoto, T.; Matsuoka, J.; Nasu, H. X-ray diffraction of silica gels made by sol-gel method under different conditions. *J. Non Cryst. Solids* **1998**, *240*, 202–211. [CrossRef]
57. García-Cerda, L.A.; Mendoza-González, O.; Pérez-Robles, J.F.; González-Hernández, J. Structural characterization and properties of colloidal silica coatings on copper substrates. *Mater. Lett.* **2002**, *56*, 450–453. [CrossRef]
58. Hagiwara, Y.; Shimojima, A.; Kuroda, K. Alkoxysilylated-derivatives of double-four-ring silicate as novel building blocks of silica-based materials. *Chem. Mater.* **2008**, *20*, 1147–1153. [CrossRef]
59. Nowacka, M.; Kowalewska, A.; Makowski, T. Structural studies on ladder phenylsilsesquioxane oligomers formed by polycondensation of cyclotetrasiloxanetetraols. *Polymer* **2016**, *87*, 81–89. [CrossRef]
60. Ospino, I.; Luquin, A.; Jiménez-Ruiz, M.; Pérez-Landazábal, J.I.; Recarte, V.; Echeverría, J.C.; Laguna, M.; Urtasun, A.A.; Garrido, J.J. Computational Modeling and Inelastic Neutron Scattering Contributions to the Study of Methyl-silica Xerogels: A Combined Theoretical and Experimental Analysis. *J. Phys. Chem. C* **2017**, *121*, 22836–22845. [CrossRef]
61. Handke, M.; Jastrzębski, W. Vibrational spectroscopy of the ring structures in silicates and siloxanes. *J. Mol. Struct.* **2004**, *704*, 63–69. [CrossRef]
62. Shi, Y.; Neuefeind, J.; Ma, D.; Page, K.; Lamberson, L.A.; Smith, N.J.; Tandia, A.; Song, A.P. Ring size distribution in silicate glasses revealed by neutron scattering first sharp diffraction peak analysis. *J. Non Cryst. Solids* **2019**, *516*, 71–81. [CrossRef]

63. Tan, C.Z.; Arndt, J. Interaction of longitudinal and transverse optic modes in silica glass. *J. Chem. Phys.* **2000**, *112*, 5970–5974. [CrossRef]
64. Caresani, J.R.; Lattuada, R.M.; Radtke, C.; Dos Santos, J.H.Z. Attempts made to heterogenize MAO via encapsulation within silica through a non-hydrolytic sol-gel process. *Powder Technol.* **2014**, *252*, 56–64. [CrossRef]
65. Choi, S.S.; Lee, A.S.; Lee, H.S.; Baek, K.Y.; Choi, D.H.; Hwang, S.S. Synthesis and characterization of ladder-like structured polysilsesquioxane with carbazole group. *Macromol. Res.* **2011**, *19*, 261–265. [CrossRef]
66. Gallardo, J.; Durán, A.; Di Martino, D.; Almeida, R.M. Structure of inorganic and hybrid SiO2 sol-gel coatings studied by variable incidence infrared spectroscopy. *J. Non Cryst. Solids* **2002**, *298*, 219–225. [CrossRef]